Reexamining cluster radioactivity in trans-lead nuclei with consideration of specific density distributions in daughter nuclei and clusters

Yibin Qian,[1,2,*] Zhongzhou Ren,[2,3,4,†] and Dongdong Ni[5]

[1]*Department of Applied Physics, Nanjing University of Science and Technology, Nanjing 210094, China*
[2]*Key Laboratory of Modern Acoustics and Department of Physics, Nanjing University, Nanjing 210093, China*
[3]*Kavli Institute for Theoretical Physics China, Beijing 100190, China*
[4]*Center of Theoretical Nuclear Physics, National Laboratory of Heavy-Ion Accelerator, Lanzhou 730000, China*
[5]*Space Science Institute, Macau University of Science and Technology, Macau 999078, China*

(Received 13 June 2016; revised manuscript received 13 July 2016; published 10 August 2016)

We further investigate the cluster emission from heavy nuclei beyond the lead region in the framework of the preformed cluster model. The refined cluster-core potential is constructed by the double-folding integral of the density distributions of the daughter nucleus and the emitted cluster, where the radius or the diffuseness parameter in the Fermi density distribution formula is determined according to the available experimental data on the charge radii and the neutron skin thickness. The Schrödinger equation of the cluster-daughter relative motion is then solved within the outgoing Coulomb wave-function boundary conditions to obtain the decay width. It is found that the present decay width of cluster emitters is clearly enhanced as compared to that in the previous case, which involved the fixed parametrization for the density distributions of daughter nuclei and clusters. Among the whole procedure, the nuclear deformation of clusters is also introduced into the calculations, and the degree of its influence on the final decay half-life is checked to some extent. Moreover, the effect from the bubble density distribution of clusters on the final decay width is carefully discussed by using the central depressed distribution.

DOI: 10.1103/PhysRevC.94.024315

I. INTRODUCTION

Since the discovery of radioactivity by Becquerel in 1896, nuclear physics has entered into the field of natural science. Subsequently, at the initial stage of nuclear physics, α decay was identified and recognized in a series of experiments. On the other side, unstable heavy nuclei or superheavy nuclei would also decay via fission (such as spontaneous fission) to the stable products. As the intermediate case between the abovementioned disintegration modes, heavier cluster emissions were first conjectured to exist in the 1980s. Based on the superasymmetric fission model (SAFM), Sándulescu, Poenaru, and Greiner [1] theoretically predicted this new kind of radioactive mode, triggered by the strong interaction and Coulomb interaction as well. Lu *et al*. [2] in particular indicated the possibility of carbon emission and the most potential emitters, ^{223,224}Ra. Very impressively, this phenomenon, ^{14}C emission from ^{223}Ra, was really and truly confirmed in the experiment proposed by Rose and Jones 4 yr later [3]. Since then, a great deal of effort has been devoted to this fascinating subject, with regard to both the experimental and theoretical aspects [4–6]. Up to now, more than 20 cluster emissions in various actinide isotopes, decaying to the doubly magic nucleus ^{208}Pb or its neighboring nuclei, have been discovered and reported via the continuous detection of such a peculiar and extremely rare decay mode [4,5]. Moreover, it is of great interest to denote that the concept of heavy-particle emission was recently expanded to allow emission of quite heavier clusters ($Z_c > 28$) from superheavy elements and daughter nuclei around the doubly magic nucleus ^{208}Pb, implying the possibility of another decay mechanism of superheavy nuclei [7,8]. This speculation stimulated the renewed interest in cluster radioactivity to some extent as well.

As is known to all, the spontaneously emitted particle in cluster decay is heavier than an α particle but lighter than the lightest fragment in nuclear fission. In this sense, it appears to be natural and straightforward to deal with the cluster emission from two aspects, namely, the fissionlike theory [1,7–14] and the α-like theory [15–23]. Within the former picture, the decay process is treated as a consecutive evolution of geometrical shapes and the formation of clusters is considered to be involved in the adiabatic rearrangement of parent nuclei. Besides the (analytical) SAFM method actually belonging to this category [7–9], the generalized liquid-drop model has been previously conducted to describe the cluster emission, where the macroscopic deformation energy plus the empirical microscopic correction was employed to give the potential barrier [12]. Recently, Denisov [13] combined the extended Thomas-Fermi approach accompanied by the microscopic shell correction with Skyrme and Coulomb forces to establish a multidimensional model of cluster radioactivity. In the framework of the Coulomb and proximity potentials [14], the cluster formation probability is evaluated as the penetrability through the internal part of the potential barrier, similar to the previous work of Poenaru and Greiner [9]. Meanwhile, this treatment leads to the recognition of different preferences for the type of emitted cluster in the trans-tin and the trans-lead regions. From the inverse perspective, the cluster preformation factor (P_c) can be extracted by dividing the experimental decay width by the product of the penetration probability and the

*qyibin@njust.edu.cn
†zren@nju.edu.cn

assault frequency, and the obtained values agree with previous ones reasonably well [22,23]. As for the traditional α-decay approach, the cluster is recognized to be preformed in the decaying nucleus before its penetration along with a certain preformation probability. The P_c value can be calculated either with some simply analytical assumption [20,21] or via solving the Schrödinger equation for the dynamic flow of mass and charge [17–19]. On the basis of the latter choice, the preformed cluster model (PCM) quantitatively well describes the lifetimes of cluster emitters. By introducing the effects of nuclear deformations and orientations [18], the PCM has been improved in the recent investigation. The effective cluster model, together with the simple expression of the cluster preformation factor (related with the size of the clusters and daughters), has been employed to successfully calculate half-lives of cluster radioactivity [20,21]. Moreover, detailed progress on the microscopic theory of cluster decay has been reviewed in Ref. [6] in terms of structural aspects.

In fact, no matter which approach is used, the preformation and penetration probabilities of the emitted cluster crucially depend on the type of interaction potentials between the cluster and the residual daughter [19]. Hence the accurate components and appropriate knowledge of the potential barrier are of great significance for the full understanding of this important radioactive mode. Previously, we systematically investigated the α-decay half-lives within the density-dependent cluster model, where the double-folding potential is sensitively connected with the proton and neutron density distributions of α particles and core nuclei. We have recently enhanced the density-dependent cluster model with the deduced parametrized density distribution of daughter nuclei from the experimental data of root-mean-square (rms) nuclear charge radii to discern the α decay from natural nuclides [24]. Meanwhile, inspired by the significant role of nuclear density, special attention has been paid to the influence of differences between the proton and the neutron density distributions in daughter nuclei on the α-decay half-life [25,26]. Consequently, it is quite interesting and desirable to understand the effect of the density distribution of the cluster-core system on the cluster-emission process. More strikingly, a few possible emitters appear exactly to be the candidates of bubble nuclei [27,28]. Whether the central depression in the density distribution of these clusters would bring about a large modification in the final half-life result is a rather interesting subject and is investigated in the following. Moreover, these daughter nuclei in cluster emissions are just around the typical nucleus ^{208}Pb, and there are available experimental data on the neutron skin in addition to plenty of data on the charge radii [29–33]. This actually provides a very suitable condition for us to obtain the specific parameters in the density distribution expression according to the experimental data instead of the artificial selection. In the next section, we give a brief overview of the theoretical model, especially of the density distribution of daughters and clusters. A series of calculated results including the detailed comparison of different cases is presented in Sec. III, and the effect of deformation in clusters is somewhat discussed as well. A summary and sequential conclusions are given in Sec. IV.

II. THEORETICAL APPROACH

A. The cluster-core system within the density-dependent cluster model

After the cluster is assumed to be preformed in the decaying nucleus, the parent nucleus can be considered as a two-body system consisting of the cluster interacting with the daughter nucleus. There is no doubt that the interaction potential between the two ingredients is the initial and crucial input for the half-life calculation of cluster emitters. In the present model, the Coulomb potential of the cluster-core system is obtained by double-folding integrating the proton density distributions of clusters and daughters and the standard proton-proton Coulomb interaction. In contrast, the nuclear potential is constructed by the double-folding integral of the respective density distributions of the cluster and the core nucleus and the effective nucleon-nucleon (NN) interaction [24]:

$$V_N(\mathbf{r}) = \iint d\mathbf{r_1} d\mathbf{r_2} \left[\rho_1^n(\mathbf{r_1}) + \rho_1^p(\mathbf{r_1})\right]\left[\rho_2^n(\mathbf{r_2}) + \rho_2^p(\mathbf{r_2})\right] \times \upsilon(\mathbf{s} = |\mathbf{r_2} + \mathbf{r} - \mathbf{r_1}|), \tag{1}$$

where r is the separation distance between the mass centers of the cluster and the daughter nucleus. As far as the nuclear part is concerned, the effective NN interaction is chosen as the popular M3Y-Reid type interaction, which has been successfully applied in radioactivity studies [20,21,23] and nuclear reaction calculations [34,35]. This specific form including two direct terms with different ranges plus an exchange part, introduced by Satchler and Love [34], is given by

$$\upsilon(\mathbf{s}) = 7999\frac{\exp(-4s)}{4s} - 2134\frac{\exp(-2.5s)}{2.5s} + J_{00}(E_c)\delta(\mathbf{s}), \tag{2}$$

where the zero-range potential $J_{00}(E_c)$ denoting the single-nucleon exchange effect is written as

$$J_{00}(E_c) = -276[1 - (0.005E_c/A_c)], \tag{3}$$

with the kinetic energy E_c and the mass number A_c of the cluster, to ensure the antisymmetrization of identical particles in the cluster and the core nucleus to some extent. The density distribution of the daughter nucleus (ρ_1) and the cluster (ρ_2) is depicted via the widely used two-parameter Fermi (2pF) form,

$$\rho_{1,2}^{\xi}(r_{1,2}) = \frac{\rho_0^{\xi}}{1 + \exp\left(\frac{r_{1,2} - R_{1/2}^{\xi}}{a^{\xi}}\right)}, \tag{4}$$

where ξ is p or n, and the ρ_0^{ξ} is determined by integrating the density distribution equivalent to the proton number or the neutron number of the corresponding nucleus. The half-density radius $R_{1/2}^{\xi}$ is related to the mass number of the cluster and the daughter, $R_{1/2}^{\xi} = c^{\xi} A_{1,2}^{1/3}$. As a consequence, the rms proton and neutron radii of the cluster or the daughter nucleus can be obtained by

$$R^{\xi} \equiv \sqrt{\langle r^2 \rangle} = \left[\frac{\int \rho(r) r^4 dr}{\int \rho(r) r^2 dr}\right]^{1/2}, \tag{5}$$

and the details about the choice of the parameter c^{ξ} and the diffuseness a^{ξ} are presented in the next subsection. Once the nuclear and Coulomb interaction potentials are conducted via the above procedure, the following process proceeds by solving the stationary Schrödinger equation, aiming at the relative motion of the emitted cluster with respect to the core nucleus,

$$\left(-\frac{\hbar^2}{2\mu}\frac{d^2}{dr^2}+V(r)\right)\varphi_{n\ell j}(r)=Q\varphi_{n\ell j}(r). \tag{6}$$

Here the total interaction potential $V(r)$, composed of the attractive nuclear term, the repulsive Coulomb term, and the additional centrifugal part, is written as

$$V(r)=\lambda V_N(r)+V_C(r)+\frac{\ell(\ell+1)\hbar^2}{2\mu r^2}, \tag{7}$$

where μ is the reduced mass of the cluster-core system measured in the unit of the nucleon mass $\mu=\frac{A_cA_d}{A_c+A_d}$, and ℓ is the angular momentum carried by the emitted cluster. Because the decay energy Q is very sensitive to the final half-life calculation and its accuracy cannot be sufficiently predicted in a given potential, the renormalization factor λ of the nuclear potential is set to adjust the experimental Q value. In the meantime, the quantum number n, namely, the number of the internal nodes in the radial wave function, is chosen according to the Wildermuth and Tang condition [36],

$$G=2n+L=\sum_{i=1}^{A_c}\left(g_i^{A_c+A_d}-g_i^{A_c}\right), \tag{8}$$

to satisfy the main effect of the Pauli principle besides the partial absorbtion of this effect into the cluster-core nuclear potential. In the above expression, $g_i^{A_c+A_d}$ are the oscillator quantum numbers of the ingredient nucleon in the cluster, and their values are confined to guarantee the cluster completely outside the shell occupied by the core nucleus. The $g_i^{A_c}$ are the interior quantum numbers of the A_c nucleons for the cluster in the shell model. In this way, the quantum numbers of the cluster are related to the shell-model quantum numbers of these nucleons forming the cluster. Here we take $g_i=6$ for nucleons beyond the $N=126$ neutron shell closure, $g_i=5$ for nucleons with $82<Z$ and $N\leqslant 126$, and $g_i=4$ in the region of $50<Z$ and $N\leqslant 82$. Subsequently, the quasibound solution $\varphi_{n\ell j}(r)$ is achieved with the outgoing Coulomb wave-function boundary condition due to the dominant position of the Coulomb and centrifugal potentials [21,37]:

$$\varphi_{n\ell j}(r)=N_{\ell j}[G_\ell(kr)+iF_\ell(kr)], \tag{9}$$

where $N_{\ell j}$ is the normalization constant, and G_ℓ and F_ℓ are, respectively, the irregular and regular Coulomb wave functions with the wave number $k=\sqrt{2\mu Q}/\hbar$. The probability rate per second that the cluster goes through a surface element is $P_{\ell j}=|\varphi_{n\ell j}(r)|^2/r^2 v dS$, where the velocity v of the cluster at large distances is $v=\hbar k/\mu$ and $dS=r^2\sin\theta d\theta d\phi$. Provided that $|G_{\ell j}+iF_{\ell j}|^2=1$ at large distances and that the inner and outer solutions should be matched at the large distance R beyond the range of the nuclear potential, one can obtain the decay width by integrating $P_{\ell j}$ over the angles,

$$\Gamma=\frac{\hbar^2k}{\mu}|N_{\ell j}|^2=\frac{\hbar^2k}{\mu}\frac{|\varphi_{n\ell j}(R)|^2}{G_\ell(kR)^2+F_\ell(kR)^2}, \tag{10}$$

which yields almost the same value regardless of the choice of R as long as it has been located in the regime with varnishing nuclear potential. It is then indispensable to include the cluster preformation factor P_c, measuring the extent to which the cluster is formed at the nuclear surface, to calculate the absolute half-life of cluster decay. The clustering phenomenon has now been considered as one basic dynamic in nuclear structure and reaction, and cluster structure in fact plays an important role not only in light nuclei [38] but also in heavy ones [39]. As mentioned before, the cluster preformation probability can be taken into account from different aspects and basements. In the present study, the P_c value can be extracted as the ratio of the experimental decay width to the calculated one via the formula $P_c=\Gamma_{\rm expt}/\Gamma_{\rm calc}$, in which the experimental decay width $\Gamma_{\rm expt}$ is related to the experimental half-life by the well-known relationship $\Gamma_{\rm expt}=\hbar\ln 2/T_{1/2}$. Based on some available experimental cases, the formation of clusters should decrease considerably in magnitude with the increasing of their size. Moreover, a given cluster can emit from different parent nuclei, somewhat requiring that the preformation factor should correlate with the size of the parent nucleus or its daughter. With these factors in mind, the cluster preformation factor is supposed to behave as follows [21]:

$$\log_{10}P_c=a\sqrt{\mu}(Z_cZ_d)^{1/2}+b, \tag{11}$$

where Z_c and Z_d are the atomic numbers of the cluster and the daughter nucleus, respectively, and the parameters a and b are to be determined. It should be noted that the objective of this article is actually focused on the effect of the density distributions of clusters and daughters on the decay width, and the P_c values are consequently expected to preform differently regarding different density distributions. As well, it is exciting to check whether the trend of P_c matches such a linear relationship, which is valuable for the description of cluster emission half-lives especially for the unknown emitters such as superheavy nuclei and the lighter nuclei beyond the tin region.

Before concentrating on the parameters involved in the daughter and cluster densities, we take into account the effect that nuclear deformation deviated from spherical symmetry has had on cluster emission. As far as available cluster decay is concerned, the daughter nucleus is mostly in the close location around the doubly magic nucleus ^{208}Pb, and these nuclei are generally spherical or near spherical. By contrast, several emitted clusters are considered to possess deformed shapes. The cluster emitter can then be figured as a system comprising a spherical daughter nucleus interacting with an axial-symmetric cluster. The deformed density distributions of clusters are taken as the 2pF form all the same, but accompanied by an orientation-dependent half-density radius,

$$R_2^{1/2}(\theta)=cA_2^{1/3}[1+\beta_2Y_{20}(\theta)+\beta_4Y_{40}(\theta)], \tag{12}$$

where β_2 and β_4 are the quadrupole and hexadecapole deformation parameters [40]. The rms nuclear radii are then

obtained as

$$R \equiv \sqrt{\langle r^2 \rangle} = \left[\frac{\iint \rho_2(r,\theta) r^4 \sin\theta dr d\theta}{\iint \rho_2(r,\theta) r^2 \sin\theta dr d\theta} \right]^{1/2}. \quad (13)$$

The orientation-dependent double-folding potential can then be evaluated via the sum of different multipole components after the multipole expansion of the deformed density is adopted (see details in Refs. [21,35] and references therein). The daughter nucleus can be in any direction with respect to the symmetrical axis of the deformed cluster, leading to a different partial decay width $\Gamma(\beta)$ depending on this orientation. Hence once $\Gamma(\beta)$ is evaluated via the abovementioned spherical situation, the final decay width can be simply reached by averaging the partial decay width all along the direction,

$$\Gamma = \int_0^{\pi/2} \Gamma(\beta) \sin\beta d\beta, \quad (14)$$

where β is the orientation angle between the spherical daughter and the symmetric axis of the cluster.

B. Parameter choice in the density distribution of clusters and daughter nuclei

In the previous studies based on the double-folding potential, the particular parameters in the 2pF formula of the density distribution are usually fixed as the constants $R_{1/2} = 1.07A^{1/3}$ fm and $a = 0.54$ fm, within which the matter radius of heavy nuclei would be approximately produced as $R_{\rm rms} \approx 1.2A^{1/3}$. Given that there have been a number of available experimental data on nuclear charge radii, it appears to be more reasonable and convincing to obtain these parameters from the experimental nuclear radii, while the crucial cluster-core system potential is quite sensitive to the density distribution. We have recently paid special attention to long-lived α-decaying nuclei considering the density distributions (2pF) of daughter nuclei in this way [24]. It has been found that the agreement between theory and experiment has improved and the predicted α-decay half-lives have been reduced particularly for several probable candidates of natural α emitters. More strikingly, it has been found that the neutron skin thickness is considerable for heavy nuclei like these daughter nuclei in cluster or α emissions. Therefore the proton and neutron density distributions should be distinguished to detect their effects on the cluster decay width. Fortunately, these daughter nuclei in cluster emissions usually possess experimental data about the nuclear charge radii and the available value of the neutron skin, offering an excellent opportunity for our following work. Meanwhile, some emitted clusters may be possible bubble nuclei and then the peculiar density distribution in their central part should receive special attention. To begin with, the proton and neutron density distributions of daughter nuclei are believed to exhibit different parameters, (c_1^p, a_1^p) and (c_1^n, a_1^n), despite the same 2pF form. Their differences are deduced from the the neutron skin thickness, defined by the discrepancy between the rms neutron radius and the rms proton radius: $\Delta R_{np} = R_n - R_p$. As mentioned in Refs. [30,31], there are two extreme cases for the density distribution, namely, the "neutron skin" type with $c^n > c^p$ and $a^n = a^p$ and the "neutron halo" type with $c^n = c^p$ and $a^n > a^p$. It should be noted that these experiments in antiprotonic atoms preferentially support the latter situation of "neutron halo" density distribution. In contrast, we find that the final half-lives of cluster emissions have little change within the two cases actually, which is consistent with the results in Ref. [25]. Therefore, we mainly concentrate on the halo type density distribution in the following, for the sake of convenience and clearness. In detail of this type, the diffuseness parameter in the proton density distribution of daughter nuclei is still fixed at $a_1^p = 0.54$ fm as usual, while the half-density parameter c_1^p is determined in terms of their experimental charge radii via the relationship (5). When it comes to the neutron density distribution, the diffuseness parameter a_1^n can then be obtained according to the rms neutron radius, $R_n = R_p + \Delta R_{np}$, with the same half-density parameter $c_1^n = c_1^p$. By contrast, the situation in light nuclei, i.e., these emitted clusters, is assumed to be simpler considering that the deviation between the proton and neutron numbers is small and their values are small as well. Hence the proton and neutron density distributions are assumed to behave in the same 2pF along with the identical parameters in the present work. In addition, the introduction of this difference in the model is convenient and direct once we receive more information on the neutron skin of clusters.

Nowadays, rms nuclear charge radii and corresponding charge distributions have been accumulated for a great deal of nuclei all over the nuclear chart, due to various effective experimental methods such as electron scattering, muonic atom spectra, optical and K_α x-ray isotope shifts, etc. [29]. On the contrary, the measurement on neutron rms radii is quite restricted along with limited experimental data, and furthermore the uncertainties of extracted neutron radii are much more than those of charge radii even up to an order of magnitude. Even if the typical nucleus ^{208}Pb is concerned, the extracted value of the neutron skin is still accompanied by large error bars. For instance, its ΔR_{np} value is confined to $0.33^{+0.16}_{-0.18}$ fm through the parity-violating electron scattering performed by the lead radius (PREX) collaboration of JLab, and the neutron skin thickness is fixed as $\Delta R_{np} = 0.15 \pm 0.03(\text{stat.})^{+0.01}_{-0.03}(\text{sys.})$ fm from coherent pion photoproduction cross sections. Regardless of the large statistical errors, the ΔR_{np} is found to be in a linear relationship with the neutron-proton asymmetry term $I = (N - Z)/A$ on the basis of experimental values of 26 stable nuclei from the antiprotonic atoms, which agrees well with other theoretical calculations [30,31]. The specific expression of this linear relationship is $\Delta R_{np} = (0.90 \pm 0.15)I + (-0.03 \pm 0.02)$ fm, and this formula populates the $\Delta R_{np} = 0.160(52)$ fm for ^{208}Pb, being consistent with both the available experiments and theoretical reports. In the present calculations, we adopt this concise and reliable formula to evaluate the neutron skin thickness for these daughter nuclei involved in the cluster emissions.

To clearly demonstrate our calculations, the concerned cases are classified in detail as follows.

(1) The half-density radius parameter c and the diffuseness a in the proton and neutron density distributions of both clusters and daughter nuclei are all fixed at identical

constants ($\Delta R_{np} = 0$). This case is denoted as "calc 1."

(2) These specific parameters in the density distribution of daughter nuclei are determined by the aforementioned rule of the neutron halo type, while those in clusters are still taken as the fixed values. This case is denoted as "calc 2."

(3) This case is the same as calc 2 but the parameters in the density distribution of clusters are obtained according to their charge radii. This case is denoted as "calc 3."

Through the detailed comparison of calculated results in the three different choices (regarding the density distribution of clusters and daughter nuclei), the effect of the density distribution on cluster emissions can be deeply investigated. Moreover, a three-parameter Fermi (3pF) formula is employed to further describe the density distribution of clusters:

$$\rho_2(r_2) = \frac{\rho_0\left(1 + \omega r_2^2/R_{1/2}^2\right)}{1 + \exp\left(\frac{r_2 - R_{1/2}}{a}\right)}, \tag{15}$$

for detecting the influence of the central depression of density in clusters on the cluster decay. Here ω (>0) affects the central density, and the degree of depression in the central density increases with the ω value increasing. For a better insight, the depression degree, i.e., the quantitative bubble effect, is defined to measure how the central density is depressed:

$$D = \frac{\rho_{\max} - \rho_{\text{cent}}}{\rho_{\max}} \times 100\%, \tag{16}$$

where $\rho_{\max}$ and ρ_{cent}, respectively, represent the maximum density and the central density.

III. NUMERICAL RESULTS AND DISCUSSION

As we all know, the cluster-core potential is pivotal for calculating the decay width of cluster emitters. Consequently, it is quite interesting to directly check the change of total potential along with the different cases of density distribution in daughter nuclei and clusters. Here we take the cluster radioactivity $^{222}\text{Ra} \rightarrow {}^{208}\text{Pb} + {}^{14}\text{C}$ for illustration, involving a spherical cluster ($\beta_2 = \beta_4 = 0$) and then bringing an orientation-independent potential. Figure 1 presents the total interaction $\lambda V_N + V_C$, including the situation in the neutron skin type density distribution of ^{208}Pb to compare with the neutron halo case as well. In the neutron skin case, the diffuseness of proton and neutron densities is set as the same value $a^p = a^n = 0.54$ fm, while the radius parameters c^p and c^n are separately determined from the rms proton and neutron radii. On one hand, provided that the neutron skin thickness brings a more expanded neutron distribution, the potential well of the cluster-core system would be wider and the interior potential would be reduced as well. Indeed, from this figure, one can see that the total potential of case calc 1 with $\Delta R_{np} = 0$ is the deepest in the inner region, but gradually ascends beyond those in other cases in the middle part of the barrier and slightly locates above the other lines in the prefragmentation region before the coincidence of all potentials. Additionally, this situation would be compensated by the introduction of the deduced density distribution of the cluster from the experimental nuclear radii, due to a little more compact density of the cluster, as displayed by the magenta line in Fig. 1. In the meantime, the total potential of the neutron halo case is located below that of the skin case in the beginning region similarly due to the more extended neutron distribution in the former one, but they would generally follow the same

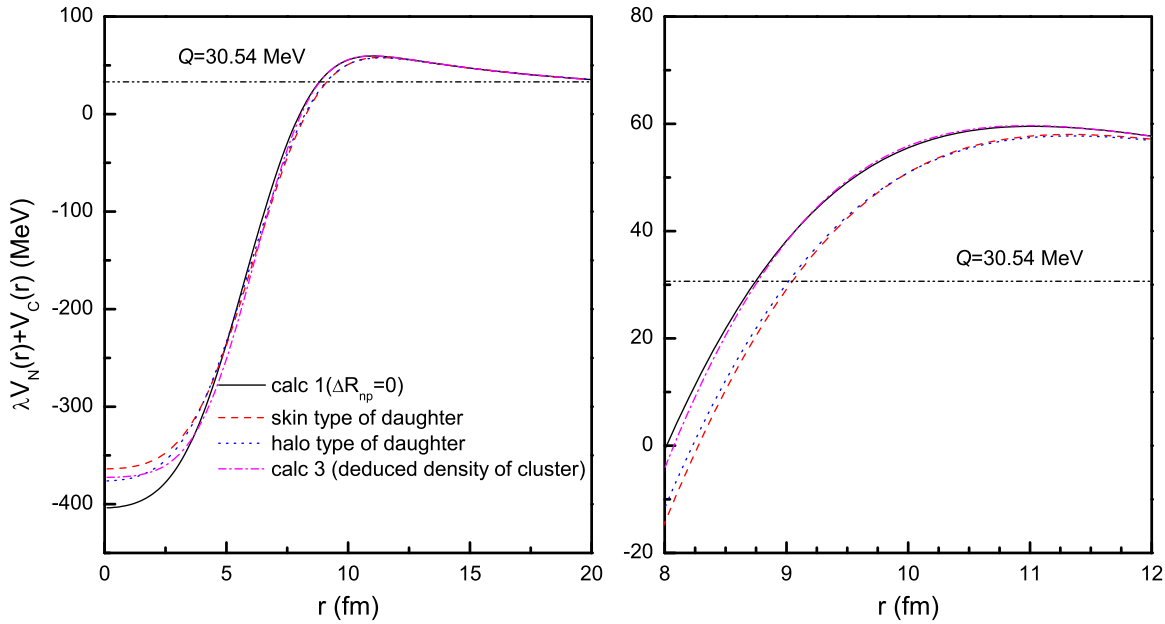

FIG. 1. Schematic diagram of the total interaction potential $V(r) = \lambda V_N(r) + V_C(r)$ between the daughter ^{208}Pb and the cluster ^{14}C for the cluster emitter ^{222}Ra. The black line denotes the case calc 1 with $\Delta R_{np} = 0$, the red dashed line presents the neutron skin type distribution with $\Delta R_{np} = 0.160$ fm, the blue dotted line gives the halo type case, while the magenta dash-dotted line indicates the halo daughter with the deduced density distribution of clusters (calc 3). The magnified version of the potential in the range of $r = 8$–12 fm is plotted in the right panel for clarity.

line in other regimes. On the other hand, the barrier penetration probability of the cluster depends on the barrier beyond the the decay energy Q in an exponential law. Meanwhile, this primary area in case calc 1, without considering the neutron skin, is comparable to that in case calc 3 but larger than those in cases of neutron skin or halo type daughter, which has been particularly shown in the right panel of Fig. 1. This indicates that the decay width of calc 1 should be clearly reduced as compared to that in either the halo or the skin case with reconsideration of density distribution in the daughter nuclei, which will be specifically examined in the representation of calculated results. The extent of this reduction would be decreased with the weight of specific density in the cluster (calc 3), which is further presented in the following calculated results. It is important to point out that the two potential curves in halo and skin types of daughter nuclei basically coincide except for the initial inner region, which has little to do with the penetration process. As a result, it appears to be reasonable and reliable to approve the claim that the final decay widths in the two cases are quite close to each other, and we then just give the calculated results from the preferential halo treatment of the neutron skin thickness in experiments [30,31]. Next, we turn to the detailed calculation of cluster emissions including even-even and odd-A parent nuclei.

Table I represents the detailed calculated results within the three aforementioned cases with different considerations of density in daughters and clusters. The first column denotes each cluster decay, and the corresponding decay energy [41] is given in the second column. The extracted $P_c = \Gamma_{\rm expt}/\Gamma_{\rm calc}$ values within cases calc 1, calc 2, and calc 3, in the logarithm scale, are respectively presented in the following three columns. The experimental rms charge radii of a few clusters are unavailable at present. Instead, they are estimated by the simple relationship $R = (c_0 + c_1 A^{-2/3} + c_3 A^{-4/3})A^{1/3}$ based on the systematics of the available data, where the parameters are $c_0 = 0.9071$ fm, $c_1 = 1.105$ fm, and $c_2 = -0.548$ fm. As one can see, $\log_{10} P_c^{\rm calc2}$ is much smaller as compared to $\log_{10} P_c^{\rm calc1}$, which implies that the consideration of the neutron skin effect and the deduced density distribution would bring a quite distinct enhancement of the decay width. After the density distribution of clusters is also taken into account from the experimental nuclear radii, the decay width is diminished to a certain extent as can be seen by the comparison of calc 2 and calc 3 and their corresponding potentials in Fig. 1, leading to the bounce of the extracted P_c value. However, the decay width of cluster emissions generally increases as long as the densities of daughter nuclei and emitted clusters are deduced from the available experimental facts about the rms proton and neutron radii instead of previous artificial choices without considering the neutron skin. In other words, the preformation of clusters at the surface of the parent nucleus may be more difficult in contrast with previous recognitions. To obtain an overall picture, we also plot the $\log_{10} P_c$ versus the quantity $\sqrt{\mu}(Z_c Z_d)^{1/2}$ of Eq. (11) in Fig. 2, divided by even-even and odd-A parent nuclei. More interestingly, it is quite straightforward to examine whether there exists a linear relationship between these two quantities. As expected, the extracted P_c values in general locate around each fitted line. Moreover, the preformation factor of even-even nuclei appears to be higher than that of odd-A nuclei for one given cluster, which can be understood by the hinderance effect from the unpaired nucleons. Please note that even if the parent nucleus involves the same odd nucleons, the situations may not always be alike due to the different cases of emitted clusters, i.e., even-even and odd-A clusters [21], which may cause the agreement between the extracted P_c value and the line, Eq. (11), of odd-A parent nuclei to be relatively worse than that of even-even nuclei. Referring to the deformed shape of clusters, it is inviting to check the sensitivity of the calculated half-lives to the deformation of clusters. In Fig. 3 we take the cluster emission $^{228}\mathrm{Th} \rightarrow {}^{208}\mathrm{Pb} + {}^{20}\mathrm{O}$, for example, in which the ratio of the calculated half-life $T_{1/2}^{\beta_2}$ in one certain β_2 value to that in the spherical case $T_{1/2}^{0}$ (namely, $\beta_2 = 0$) is plotted versus the quadrupole deformation parameter β_2 of ^{20}O in the range of -0.35–0.30. To check the reliability of the present treatment of the nuclear deformation [i.e., Eq. (14)], our results are also compared with those from the exact coupled-channel method. Here we take the case of a large deformation value as the illustration, the present ratios $T_{1/2}^{\beta_2}/T_{1/2}^{0}$ are separately 0.91 and 0.80 when the β_2 values of the cluster ^{20}O are 0.2 and 0.3, respectively, while the ratios in the coupled-channel analysis are correspondingly 0.90 and 0.79. Obviously, these two calculations are consistent with each other, which validates the present approach to a great extent. From this figure, one can see that the decreasing speed of the calculated half-life with the deformation parameter is slightly larger in the prolate shape region of the cluster ($\beta_2 > 0$) as compared to that in

TABLE I. Comparison of calculated results from various cases with different density distributions of daughter nuclei and clusters, as mentioned in the previous section. Note that the logarithm of the P_c values, extracted by $\Gamma_{\rm expt}/\Gamma_{\rm calc}$, is actually directly connected with the calculated decay width. Hence the presented P_c values could indicate the effect of density distributions on cluster decay.

Transition	Q (MeV)	$\log_{10} P_c^{\rm calc1}$	$\log_{10} P_c^{\rm calc2}$	$\log_{10} P_c^{\rm calc3}$
$^{221}\mathrm{Fr} \rightarrow {}^{207}\mathrm{Tl} + {}^{14}\mathrm{C}$	31.29	−4.30	−5.59	−4.26
$^{221}\mathrm{Ra} \rightarrow {}^{207}\mathrm{Pb} + {}^{14}\mathrm{C}$	32.40	−4.28	−5.59	−4.26
$^{222}\mathrm{Ra} \rightarrow {}^{208}\mathrm{Pb} + {}^{14}\mathrm{C}$	33.05	−3.60	−4.91	−3.58
$^{223}\mathrm{Ra} \rightarrow {}^{209}\mathrm{Pb} + {}^{14}\mathrm{C}$	31.83	−4.94	−6.29	−4.95
$^{224}\mathrm{Ra} \rightarrow {}^{210}\mathrm{Pb} + {}^{14}\mathrm{C}$	30.54	−3.43	−4.82	−3.49
$^{226}\mathrm{Ra} \rightarrow {}^{212}\mathrm{Pb} + {}^{14}\mathrm{C}$	28.20	−3.64	−5.10	−3.76
$^{228}\mathrm{Th} \rightarrow {}^{208}\mathrm{Pb} + {}^{20}\mathrm{O}$	44.72	−4.06	−5.93	−4.72
$^{230}\mathrm{Th} \rightarrow {}^{206}\mathrm{Hg} + {}^{24}\mathrm{Ne}$	57.76	−5.20	−7.44	−5.59
$^{231}\mathrm{Pa} \rightarrow {}^{208}\mathrm{Pb} + {}^{23}\mathrm{F}$	51.84	−7.18	−9.25	−7.88
$^{231}\mathrm{Pa} \rightarrow {}^{207}\mathrm{Tl} + {}^{24}\mathrm{Ne}$	60.41	−6.33	−8.47	−6.62
$^{230}\mathrm{U} \rightarrow {}^{208}\mathrm{Pb} + {}^{22}\mathrm{Ne}$	61.39	−4.90	−6.91	−5.27
$^{232}\mathrm{U} \rightarrow {}^{208}\mathrm{Pb} + {}^{24}\mathrm{Ne}$	62.31	−5.35	−7.58	−5.72
$^{233}\mathrm{U} \rightarrow {}^{209}\mathrm{Pb} + {}^{24}\mathrm{Ne}$	60.49	−7.14	−9.40	−7.53
$^{233}\mathrm{U} \rightarrow {}^{208}\mathrm{Pb} + {}^{25}\mathrm{Ne}$	60.78	−6.36	−8.88	−7.21
$^{234}\mathrm{U} \rightarrow {}^{210}\mathrm{Pb} + {}^{24}\mathrm{Ne}$	58.83	−5.59	−7.94	−6.08
$^{234}\mathrm{U} \rightarrow {}^{208}\mathrm{Pb} + {}^{26}\mathrm{Ne}$	59.47	−4.99	−7.18	−5.28
$^{234}\mathrm{U} \rightarrow {}^{206}\mathrm{Hg} + {}^{28}\mathrm{Mg}$	74.11	−6.11	−8.39	−6.61
$^{236}\mathrm{Pu} \rightarrow {}^{208}\mathrm{Pb} + {}^{28}\mathrm{Mg}$	79.67	−6.81	−9.05	−7.25
$^{238}\mathrm{Pu} \rightarrow {}^{210}\mathrm{Pb} + {}^{28}\mathrm{Mg}$	75.91	−6.02	−8.35	−6.56
$^{238}\mathrm{Pu} \rightarrow {}^{208}\mathrm{Pb} + {}^{30}\mathrm{Mg}$	76.82	−6.35	−8.48	−7.00

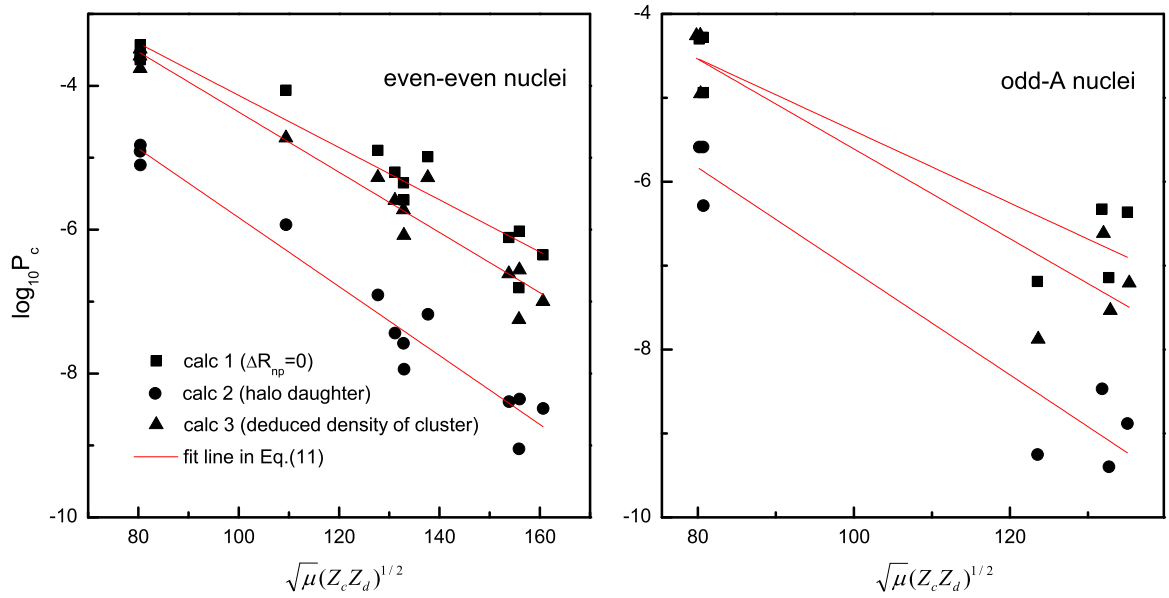

FIG. 2. Variation of the extracted P_c value with the quantity $\sqrt{\mu}(Z_cZ_d)^{1/2}$ including the results in the three cases and the correspondingly fitted line, which are separated as even-even nuclei and odd-A nuclei.

the oblate case. In addition, it is clear that the calculated half-life would be somewhat reduced with the introduction of the deformation effect of the cluster, and the declination degree could be easily discerned from this figure. One can see that the increasing of the β_2 value of ^{20}O from 0 (spherical) to 0.30 could bring an approximate 20% reduction in the calculated half-life $T_{1/2}$.

In the end, special attention should be paid to the role of the bubble phenomenon of clusters being played in the calculation of the decay width for cluster radioactivity. According to the theoretical calculations in Ref. [27], ^{20,22}O are strongly recommended to be the candidates for the bubble nuclei, which hold quite obvious depressed density in the central region. On the other hand, the 3pF formula has been employed to depict the charge density distribution and the subsequential charge form factors of light nuclei [28]. Moreover, to maintain the constant rms charge radius while increasing the central depression, the 2pF distribution plus a subtraction of the Gaussian distribution was applied to present the charge density in Ref. [28]. Keeping these factors in mind, we plan to make use of the 3pF density distribution of ^{20}O [Eq. (15)], as an example, to investigate the effect of the central depression on the final decay width of cluster emitters. Differently, the half-density radius parameter $R_{1/2} = cA^{1/3}$ is determined by matching the experimental nuclear radius; meanwhile the diffuseness a is settled as 0.46 fm to maintain the positive value of $R_{1/2}$ and the positive depression in the center of cluster density. The larger the ω is, the more depressed is the central density corresponding to the larger D of Eq. (16). For one ω, the c value in the half-density radius is obtained in terms of the constant measured radius. We find that the calculated half-life (with $P_c = 1$) increases more sharply with the enhanced ω value at the beginning, and the increasing trend slows down after the ω value reaches one certain value, which is clearly shown in Fig. 4. The corresponding central depression degree D is illustrated in the right panel of the figure as well. In detail, when the depression D achieves about the evaluated value of 20% in Ref. [27], the calculated half-life would increase about 10% as compared to that without deliberation of the central depression. In combination with the fact that the calculated decay widths generally remain unchanged with two different extreme choices of the daughter density, namely, the neutron skin and neutron halo types, it may conclude that as long as the nuclear radii of the daughter and the cluster are fixed, the final decay width of cluster emission is not quite sensitive to the specific form of density distribution.

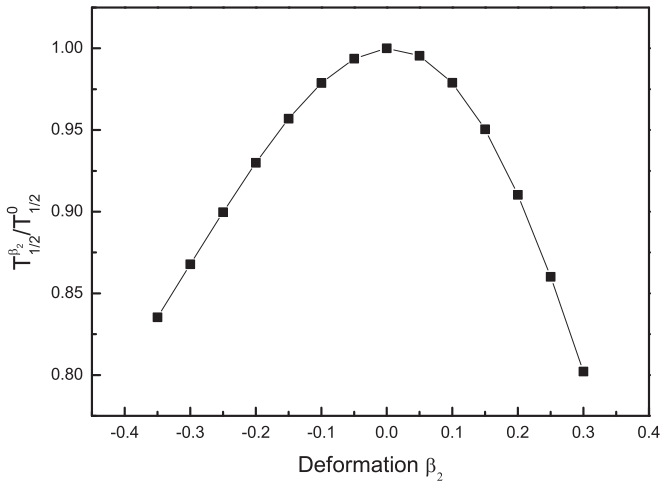

FIG. 3. The ratio of the calculated half-life to that in the spherical case, denoted as $T^{\beta_2}_{1/2}/T^0_{1/2}$, varies with the change of deformation parameters β_2 of ^{20}O in the cluster emission of ^{228}Th.

IV. SUMMARY

To conclude, we systematically study the effect of different density distributions of daughter nuclei and clusters on cluster decay. The double-folding model is employed to establish

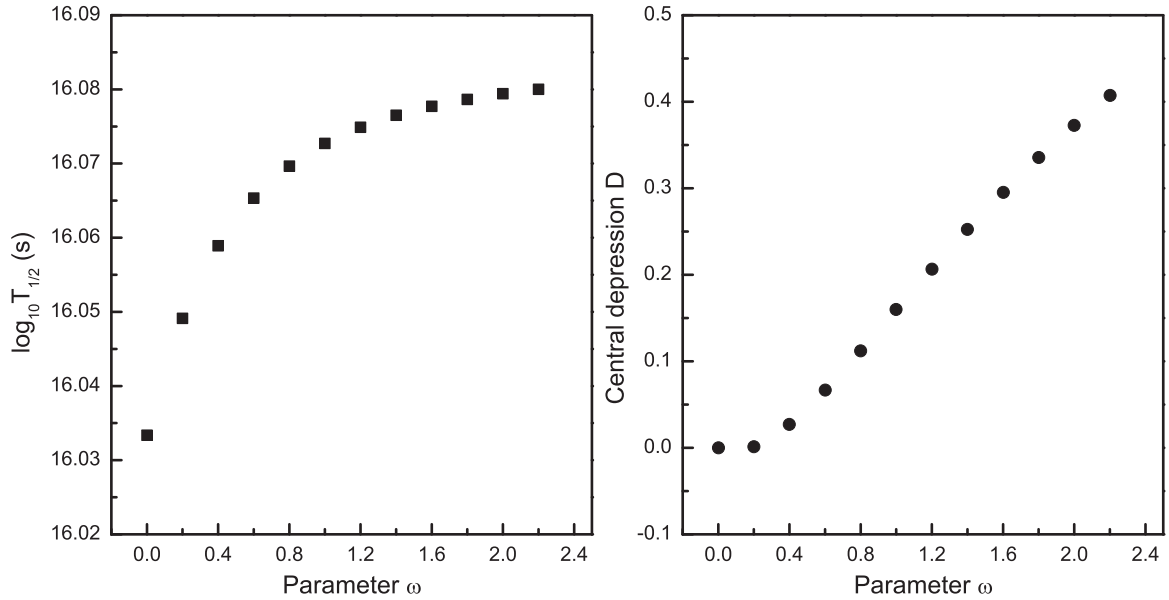

FIG. 4. Variety of calculated half-lives with $P_c = 1$ versus the increasing of the depression parameter ω for cluster decay $^{228}\mathrm{Th} \rightarrow {}^{208}\mathrm{Pb} + {}^{20}\mathrm{O}$, which is plotted in the left panel. Correspondingly, the central depressed degree, defined as the ratio of the deviation between the maximum and central densities to the maximum of the density, is plotted in the right panel to present a comprehensive view.

the cluster-core potential, where the specific parameters in the proton and neutron density forms are obtained from the combination of the experimental charge radii and the thickness of the neutron skin. Additionally, the nuclear deformation of clusters is somewhat considered via the deformed 2pF distribution. It is demonstrated that the calculated half-lives (with the unity P_c) of cluster emitters are reduced to a large extent once the density distribution of daughter nuclei is determined from the measured nuclear radii and especially the consideration of the neutron skin, while the introduction of deduced density in clusters somewhat offsets this reduction. Consequently, the preformation of a cluster before its penetration appears to be more difficult in contrast with previous thought. During the calculation, two extreme types of daughter distribution, i.e., neutron halo and neutron skin, are considered, and their resulting decay widths are actually close to each other. We have mainly presented the calculation in the neutron halo type in light of the experiments in antiprotonic atoms. Furthermore, the 3pF distribution is applied to describe the central depression of cluster density, revealing that the decay width of cluster emission could be decreased with the increasing of the depressed degree of the cluster. In general, the extracted P_c values indeed conform to the simple exponential relationship accompanied by atomic numbers of daughter nuclei and clusters as expected.

ACKNOWLEDGMENTS

This work is supported by the Natural Science Youth Fund of Jiangsu Province (Grant No. BK20150762), by the Fundamental Research Funds for the Central Universities (Grant No. 30916011339), by the National Natural Science Foundation of China (Grants No. 11375086, No. 11535004, and No. 11120101005), by the 973 National Major State Basic Research and Development Program of China (Grant No. 2013CB834400), by the Science and Technology Development Fund of Macau under Grants No. 020/2014/A1 and No. 039/2013/A2, and by a project funded by the Priority Academic Programme Development of JiangSu Higher Education Institutions (PAPD).

[1] A. Săndulescu, D. N. Poenaru, and W. Greiner, Sov. J. Part. Nucl. **11**, 528 (1980).
[2] X. T. Lu, D. X. Jiang, and Y. L. Ye, *Nuclear Physics* (Atomic Energy, Beijing, 2000), p. 127.
[3] H. J. Rose and G. A. Jones, Nature (London) **307**, 245 (1984).
[4] R. Bonetti and A. Guglielmetti, Rom. Rep. Phys. **59**, 301 (2007).
[5] A. Guglielmetti, D. Faccio, R. Bonetti *et al.*, J. Phys.: Conf. Ser. **111**, 012050 (2008).
[6] R. G. Lovas, R. J. Liotta, A. Insolia, K. Varga, and D. S. Delion, Phys. Rep. **294**, 265 (1998).
[7] D. N. Poenaru, R. A. Gherghescu, and W. Greiner, Phys. Rev. Lett. **107**, 062503 (2011); Phys. Rev. C **85**, 034615 (2012).
[8] D. N. Poenaru, M. Ivaşcu, A. Săndulescu, and W. Greiner, Phys. Rev. C **32**, 572 (1985).
[9] D. N. Poenaru and W. Greiner, Phys. Scr. **44**, 427 (1991).
[10] W. Greiner, M. Ivaşcu, D. N. Poenaru, and A. Sandulescu, Z. Phys. A **320**, 347 (1985).
[11] Y.-J. Shi and W. J. Swiatecki, Phys. Rev. Lett. **54**, 300 (1985).
[12] G. Royer, R. K. Gupta, and V. Yu. Denisov, Nucl. Phys. A **632**, 275 (1998).
[13] V. Yu. Denisov, Phys. Rev. C **88**, 044608 (2013).

[14] K. P. Santhosh, R. K. Biju, and S. Sahadevan, Nucl. Phys. A **838**, 38 (2010); **847**, 42 (2010).
[15] R. Blendowske and H. Walliser, Phys. Rev. Lett. **61**, 1930 (1988).
[16] B. Buck and A. C. Merchant, Phys. Rev. C **39**, 2097 (1989).
[17] S. S. Malik and R. K. Gupta, Phys. Rev. C **39**, 1992 (1989).
[18] S. K. Arun, R. K. Gupta, B. B. Singh, S. Kanwar, and M. K. Sharma, Phys. Rev. C **79**, 064616 (2009).
[19] R. Kumar, Phys. Rev. C **86**, 044612 (2012).
[20] Z. Ren, C. Xu, and Z. Wang, Phys. Rev. C **70**, 034304 (2004).
[21] D. Ni and Z. Ren, Phys. Rev. C **82**, 024311 (2010).
[22] H. F. Zhang, J. M. Dong, G. Royer, W. Zuo, and J. Q. Li, Phys. Rev. C **80**, 037307 (2009).
[23] G. L. Zhang and X. Y. Le, Nucl. Phys. A **848**, 292 (2010).
[24] Y. Qian and Z. Ren, Phys. Lett. B **738**, 87 (2014).
[25] D. Ni and Z. Ren, Phys. Rev. C **92**, 054322 (2015).
[26] Y. Qian and Z. Ren, J. Phys. G: Nucl. Part. Phys. **43**, 065102 (2016).
[27] A. Shukla, S. Åberg, and A. Bajpeyi, Phys. At. Nucl. **79**, 11 (2016).
[28] Y. Chu, Z. Ren, Z. Wang, and T. Dong, Phys. Rev. C **82**, 024320 (2010).
[29] I. Angeli and K. P. Marinova, At. Data Nucl. Data Tables **99**, 69 (2013).
[30] A. Trzcińska, J. Jastrzębski, P. Lubiński, F. J. Hartmann, R. Schmidt, T. von Egidy, and B. Kłos, Phys. Rev. Lett. **87**, 082501 (2001).
[31] M. Warda, X. Viñas, X. Roca-Maza, and M. Centelles, Phys. Rev. C **81**, 054309 (2010).
[32] S. Abrahamyan, Z. Ahmed, H. Albataineh *et al.*, Phys. Rev. Lett. **108**, 112502 (2012).
[33] C. M. Tarbert, D. P. Watts, D. I. Glazier *et al.*, Phys. Rev. Lett. **112**, 242502 (2014).
[34] G. R. Satchler and W. G. Love, Phys. Rep. **55**, 183 (1979).
[35] A. M. Kobos, B. A. Brown, P. E. Hodgson, G. R. Satchler, and A. Budzanowski, Nucl. Phys. A **384**, 65 (1982).
[36] K. Wildermuth and Y. C. Tang, *A Unified Theory of the Nucleus* (Academic, New York, 1997).
[37] R. J. Liotta, J. Phys.: Conf. Ser. **413**, 012012 (2013).
[38] H. Horiuchi, J. Phys. G: Nucl. Part. Phys. **37**, 064021 (2010).
[39] G. Röpke, P. Schuck, Y. Funaki, H. Horiuchi, Z. Ren, A. Tohsaki, C. Xu, T. Yamada, and B. Zhou, Phys. Rev. C **90**, 034304 (2014).
[40] P. Möller, J. R. Nix, W. D. Myers, and W. J. Swiatecki, At. Data Nucl. Data Tables **59**, 185 (1995).
[41] M. Wang, G. Audi, A. H. Wapstra, F. G. Kondev, M. MacCormick, X. Xu, and B. Pfeiffer, Chin. Phys. C **36**, 1603 (2012); G. Audi, F. G. Kondev, M. Wang, B. Pfeiffer, X. Sun, J. Blachot, and M. MacCormick, *ibid.* **36**, 1157 (2012).